# EFFECT OF NANOFILLER GEOMETRY ON THE POLYMER PHYSICAL STRUCTURE AND MECHANICAL PROPERTIES OF NANOCRYSTALLINE FE-NI ALLOY/POLYAMIDE 6 COMPOSITES

Marwa A. A. Mohamed[a, *], Diego Pedrazzoli[b], Norhan Nady[c] and Kyriaki Kalaitzidou[b,d]

[a]*Institute of Advanced Technology and New Materials, Fabrication Technology Department, City of Scientific Research and Technological Applications, New Borg El-Arab, Alexandria 21934, Egypt.*

[b]*The George W. Woodruff School of Mechanical Engineering, Georgia Institute of Technology, Atlanta, GA 30332-0405, USA.*

[c]*Institute of Advanced Technology and New Materials, Polymer Department, City of Scientific Research and Technological Applications, New Borg El-Arab, Alexandria 21934, Egypt.*

[d]*School of Materials Science and Engineering, Georgia Institute of Technology, Atlanta, GA 30332-0405, USA*

[*]*e-mail address of the corresponding author:* mmohamed@mucsat.sci.eg
marwa945@yahoo.com

**Keywords:** Fe-Ni alloy/Polyamide 6 nanocomposites; Nanofiller Geometry; Tensile properties, Structure-Property relationship.

**Abstract**

*This study reports the preparation of polyamide 6 nanocomposites (PA6 PNCs) based on nanocrystalline (nc) $Fe_{20}Ni_{80}$ alloy with two different geometries, spherical-sea urchin particles and necklace chains. The PNCs corresponding to the two alloy geometries are coded UMB2-SU and UMB2-NL, respectively. The tensile properties and physical structure of the PNCs were characterized. The results reveal that the addition of nc $Fe_{20}Ni_{80}$ particles to PA6 enhances modulus and strength at the expense of toughness and UMB2-SU PNC exhibits synergistic tensile properties as compared to UMB2-NL one. Such synergism is attributed to i) the higher dispersibility and surface area of alloy particles and ii) the higher crystallinity and lower ratio of $\gamma$-form to $\alpha$-form crystals of PA6 phase, when alloy particles assume the spherical-sea urchin geometry rather than the necklace one within the nanocomposite.*

## 1. Introduction

Nanocrystalline (nc) Fe-Ni alloy is considered of great importance for various technological applications including high-density magnetic storage devices, bimetallic temperature sensors, electromagnetic shielding and microelectromechanical systems (MEMS) [1]. The attention to this alloy is attributed to its unique mechanical and magnetic properties, low thermal expansion and good electrical conductivity [2, 3]. The potential of using nc Fe-Ni alloy as a nano-filler in polymers has been explored in our previous studies [4, 5], where the mechanical and thermomechanical properties of Fe-Ni alloy/polyamide 6 (PA6) nanocomposites were investigated in terms of compounding technique and nano-filler content. The studies revealed that the nanocomposites produced by ultrasound assisted master batch (UMB) technique are

promising, compared to the currently utilized PA6 nanocomposites in engineering applications, in which PA6 is reinforced with other nano-fillers including clay, silica and carbon nanotubes. This evidences that the novel Fe-Ni/PA6 nanocomposite can be a good candidate material for engineering applications.
Geometry (morphology) of the nanofiller is among the important parameters which have much influence on the various properties of polymer nanocomposites (PNCs). Accordingly, the goal of this study is to synthesize nc Fe-Ni alloy with different geometries via simple route and investigate the effect of alloy geometry on the overall performance of Fe-Ni alloy/PA6 PNCs. Particular focus will be given on the alteration of PA6's physical properties due to different geometries of metallic nanofiller and the tensile properties of the nanocomposites. The study has been proceeded as follows. The nc $Fe_{20}Ni_{80}$ fine particles were synthesized with two different geometries; spherical-sea urchin like particles and necklace chains, by chemical reduction of the corresponding metals' salts in aqueous solution. Then the $Fe_{20}Ni_{80}$/PA6 PNCs were prepared by compounding via UMB process followed by injection molding and their tensile properties and structural parameters were determined.

## 2. Experimental

### *2.1 Materials*

The chemicals used for the synthesis of nc $Fe_{20}Ni_{80}$ alloy were nickel chloride hexahydrate ($NiCl_2.6H_2O$, 98%) and ferrous chloride ($FeCl_2$, 99%) as sources of metal ions; hydrazine hydrate ($N_2H_4.H_2O$, 96%) as a reducing agent, sodium hydroxide (NaOH, 99%) as a catalyst and distilled water as a solvent. They were purchased from Panreac Quimica, Spain, Spectrum Chemical MFG. CORP, USA, VWR, USA, and El Nasr Pharmaceutical, Egypt, respectively. The polymer used was PA6 pellets (Tecomid® NB40 NL E). It is obtained in a sealed package from Eurotec® Engineering Plastics, Turkey. Formic acid ($HCO_2H$, 98%) and ethanol ($C_2H_5OH$, 96%) used as a solvent and a precipitant for PA6, respectively, were obtained from Chem-Lab NV, Belgium and VWR, USA, respectively.

### *2.2 Synthesis of nc $Fe_{20}Ni_{80}$ particles*

The synthesis of the nc $Fe_{20}Ni_{80}$ particles with two different geometries was done according to the protocol reported in [6]. Briefly, appropriate amounts of $FeCl_2$ and $NiCl_2.6H_2O$ were dissolved in distilled water to form aqueous solution of $Fe^{2+}$ and $Ni^{2+}$ ions. The molar ratio of $Fe^{2+}/Ni^{2+}$ was 2:8 and the total concentration of metal ions ($C_M$) was either 0.2 M or 0.6 M. The solution was vigorously stirred and heated to 90 °C. Then, a second solution of aqueous hydrazine, $N_2H_4.H_2O$, (50 wt%), and aqueous NaOH (0.1 M) was added to it. The volumetric ratio of aqueous $N_2H_4.H_2O$/NaOH solutions was 4:1. Fine black particles were precipitated as a result of the reduction reaction. The resulting particles were separated magnetically, washed repeatedly with distilled water until neutral pH and dried in vacuum at 35 °C for 7 h.

### *2.3 Preparation of $Fe_{20}Ni_{80}$/PA6 PNCs*

The PNCs samples were made in a two-step process: first the nc $Fe_{20}Ni_{80}$ particles were compounded with PA6 pellets followed by injection molding of standard dog bone samples (ASTM D638, Type V) and standard Izod bars (ASTM D256). The typical compounding process is as follows. nc $Fe_{20}Ni_{80}$ particles were compounded with half of the PA6 amount via ultrasound-assisted solution mixing (USM) to prepare concentrated USM PNCs containing 4

wt% nc $Fe_{420}Ni_{80}$. The USM PNCs were then compounded (diluted) with the rest of PA6 pellets via melt mixing to prepare UMB PNCs with 2 wt% nc $Fe_{20}Ni_{80}$.
Concentrated USM PNCs were prepared as follows. Firstly, a PA6-formic acid solution of 15 wt% PA6 concentration was prepared. Then, a second very dilute solution of PA6 in formic acid (polymer concentration ≈ 1 wt%) was prepared and nc $Fe_{20}Ni_{80}$ particles were dispersed and sonicated into it for 30 min, using ultrasonic bath. The alloy particles/PA6 ratio was 1:1 wt/wt. The particles suspension was then added to the first polymer solution, so that the concentration of polymer in the mixture was 10 wt% and the mixture was vigorously stirred for 1 h. Addition of ethanol, with the ethanol/formic acid ratio being 2:1 vol/vol, initiated the precipitation of PA6 after 30 min and led to formation of the composite powder which was completed within 30 minutes. The composite powder was separated from mixed solvent through filtration and dried in vacuum oven at 80 °C for 48 h. A DSM Micro 15 cc extruder, (vertical, co-rotating twin-screw micro extruder) and 10 cc injection molding machine were then used for compounding USM PNCs with the rest of PA6 pellets and fabrication of the UMB PNCs, respectively. The conditions used were: 240 ˚C as $T_{barrel}$ in the compounder and injection molding machine, screw speed of 150 rpm, residence time of 4 min, $T_{mold}$ of 70 ˚C and injection pressure of 0.8 MPa.
Before compounding, the PA6 pellets were dried in a vacuum oven at 80 °C for 48 h. After molding, the specimens were sealed and placed in a desiccator for a minimum of 24 h prior to testing. The detailed samples' codes are listed in Table 1.

| Sample | Code |
|---|---|
| Control PA6 | UMB0 |
| 2 wt% spherical-sea urchine $Fe_{20}Ni_{80}$/PA6 PNC | UMB2-SU |
| 2 wt% necklace $Fe_{20}Ni_{80}$/PA6 PNC | UMB2-NL |

**Table 1.** Samples' codes

### *2.4 Characterization of nc $Fe_{20}Ni_{80}$ particles*

X-ray diffraction (XRD) was employed to identify the synthesized black particles and characterize their crystallographic texture and crystal size. XRD measurements were carried out on a Shimadzu XRD-7000 diffractometer (30 kV, 30 mA; Cu Kα + Ni-filtered radiation, λ = 0.15406 nm). The 2θ range was 30-110°, at a scanning rate of 4°/min and a scanning step of 0.018°. The chemical composition was estimated by an area analysis using energy dispersive X-ray spectroscopy (EDS) equipped with the scanning electron microscope (SEM, JEOL, Model JSM 6360 LA). The morphology was investigated by scanning electron microscopy (SEM, JEOL, Model JSM 6360 LA, Japan) operating at 20 kV.

### *2.5 Characterization of $Fe_{20}Ni_{80}$/PA6 PNCs*

Tensile test was performed using an electro-mechanical testing machine (Instron 33R 4466) equipped with a 10 KN load cell, according to ASTM-D638. The test was conducted at ambient temperature with a strain rate of 1 mm/min. The reported results reflect an average of three measurements.
Modulated differential scanning calorimeter (MDSC Q200, TA instruments) was used to determine the degree of crystallinity and analyze the melting and crystallization behaviors of neat PA6 and PA6 phase in the nanocomposites. Slices had a net weight of about 8 mg were cut from the injection molded bars. The sliced samples were heated from ambient temperature to 270 °C, held at this temperature for 3 min to erase the thermal history and then cooled to 25

°C. All MDSC runs were conducted under nitrogen atmosphere with heating/cooling rates of 5 °C/min. The degree of crystallinity, $X_C$, was calculated from the enthalpy evolved during melting based on the heating scans, using the following formula [7]:

$$X_C = \frac{\Delta H_m}{(1 - \varnothing)\,\Delta H^0_m} \quad X \quad 100 \qquad (1)$$

Where $\Delta H_m$ is the apparent enthalpy of melting of sample, $\Delta H^0_m$ is the extrapolated value of the enthalpy corresponding to the melting of 100% crystalline pure PA6, which is taken as 190 J/g [8], and $\varnothing$ is weight fraction of nc $Fe_{20}Ni_{80}$ in the composites.
XRD was employed to determine the relative fraction of α and γ crystalline phases in neat PA6 and PA6 phase within the PNCs. This is important in interpreting the mechanical performance of Nylon compounds, because α-phase is much stronger and less ductile than the γ-phase [9, 10]. XRD patterns were obtained using X'Pert PRO Alfa-1 diffractometer in reflection mode (45 kV, 40 mA; Cu Kα + Ni-filtered radiation, λ = 0.154 nm). The analysis was performed on the injection molded Izod bars, at ambient temperature with a 2θ range between 8 and 80°, at a scanning rate of about 4°/min and a scanning step of 0.016°. XRD traces were de-convolved to diffraction peaks corresponding to amorphous phase and crystalline phase which is composed of α and γ crystal forms, using xPert Pro software. The percentage of γ-phase with respect to the total crystalline phase was calculated by:

$$\gamma\,(\%) = \frac{A_\gamma}{A_\alpha + A_\gamma} \quad X \quad 100 \qquad (2)$$

Where $A_\alpha$ is the area under α diffraction peaks and $A_\gamma$ is the area under γ diffraction peaks [11].

## 3. Results and Discussion

### *3.1 Characteristics of nc $Fe_{20}Ni_{80}$ particles*

The formation of nc $Fe_{20}Ni_{80}$ alloy was confirmed by the XRD and EDS analyses. The typical XRD pattern of the synthesized black particles is shown in Figure 1. According to the database of International Centre of Diffraction Data (ICDD), the five characteristic peaks for the disordered FCC γ-Fe-Ni taenite phase (2θ = 44.4°, 51.6°, 76.3°, 92.7° and 98.2), marked by the Miller indices ((111), (200), (220), (311) and (222)) respectively, are observed (ICDD card 00-038-0419). No impurity peak is found. According to EDS quantitative analysis, the atomic percentage of Ni is 79%, excluding the other elements like carbon in the supporting film and oxygen in the oxide layer formed on the particle surface. Additionally, the atomic percentage of oxygen is only 4%, indicating that the oxide layer formed on particle surface is very thin. These results reveal the formation of $Fe_{20}Ni_{80}$ alloy with high purity. The average crystallite sizes of the $Fe_{20}Ni_{80}$ alloys produced at two different $C_M$ values, were calculated based on the full width at half maximum of the (111) peak in the corresponding XRD patterns, using the Scherrer formula [12]. The data range from 14.5-16 nm, indicating that both alloys are nanocrystalline structured, regardless of the synthesis conditions.

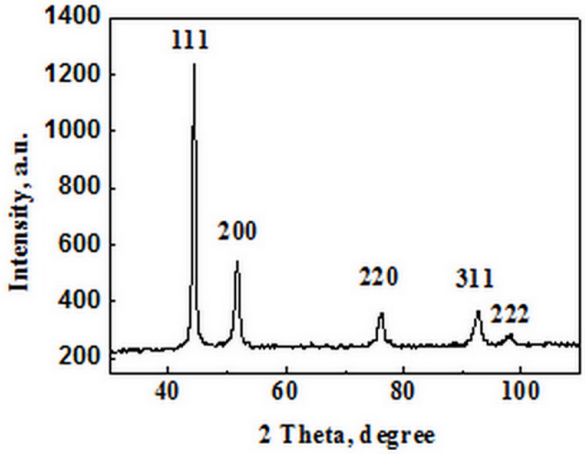


**Figure 1.** XRD pattern of the chemically synthesized black particles

SEM images of the nc $Fe_{20}Ni_{80}$ alloys, synthesized at various $C_M$ values, are presented in Figure 2. As being prepared at $C_M$ of 0.6 M, Figure 2a, the alloy exhibits spherical morphology with average diameter of about 230 nm. In addition some sea urchin-like particles are also observed. Such sea urchin-like architecture is composed of several dendrites with average diameter of about 122 nm, growing out from the surface of the spherical core, as clearly seen in high magnification image. When the $C_M$ is decreased to 0.2 M, necklace-like chains with average diameter of about 225 nm become predominant, as shown in Figure 2b. Unlike the spherical-sea urchin like particles, the necklace-like chains appear quite smooth and little bit branched, few dendritic branches can be hardly seen at high magnification.

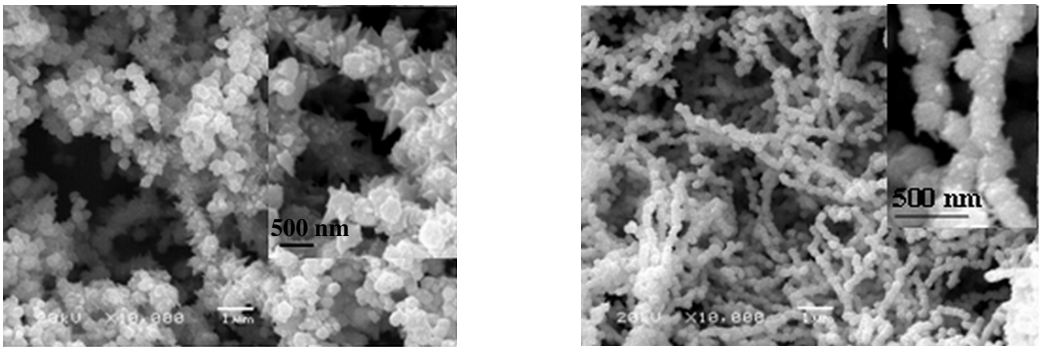


(a) (b)

**Figure 2.** SEM micrographs of nc $Fe_{20}Ni_{80}$ alloy synthesized at (a) $C_M$ of 0.6 M (spherical-sea urchin like particles) and (b) $C_M$ of 0.2 M (necklace chains).

The crucial role of $C_M$ in controlling the morphology of the alloy particles is probably because it significantly affects i) the growth rate of alloy particles and ii) the molar ratio of free $OH^-$/ ($Fe^{2+}$ and $Ni^{2+}$) ions in the reaction solution, which in turn, determine whether the evolved particle growth will be isotropic or anisotropic [6].

### *2.3 Tensile properties of $Fe_{20}Ni_{80}$/PA6 PNCs*

Figure 3 shows the typical stress-strain curves of neat PA6, UMB2-SU and UMB2-NL PNCs. The curves indicate that PA6 and the nanocomposites are ductile, because after yielding, all the samples elongated to a significant extent before breaking.

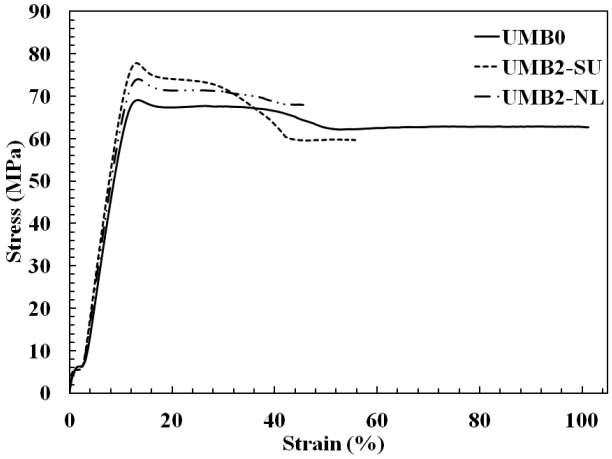


**Figure 3** Stress-strain curves of PA6 and $Fe_{20}Ni_{80}$/PA6 PNCs

A summary of the relative tensile properties of UMB2-SU PNC and UMB2-NL PNC with respect those of neat PA6, is shown in Table 2. The data reveal that the addition of nc $Fe_{20}Ni_{80}$ particles to PA6 produces a significant increase in modulus and strength at the expense of toughness. Furthermore, UMB2-SU PNC shows synergistic tensile properties as compared to UMB2-NL one. Thus the modulus and strength of UMB2-SU is improved about 13% and 12%, respectively relative to PA6 and the UMB2-NL shows 8% and 7% corresponding improvements. Moreover, UMB2-SU is more ductile than UMB2-NL, as revealed from the values of strain at break. This is probably owing to the easier dispersion of spherical-sea urchin $Fe_{20}Ni_{80}$ agglomerates into tiny particles within PA6 matrix, versus necklace $Fe_{20}Ni_{80}$ agglomerates. It is found that the magnetic dipole-dipole interaction of $Fe_{20}Ni_{80}$ alloy particles, which hinders the particles' dispersibility, substantially increases as the degree of particle anisotropy increases; coercivity of necklace $Fe_{20}Ni_{80}$ alloy measures 109 G as compared to 85 G for the alloy with spherical-sea urchin morphology [6]. In addition, the dense dendritic branches of sea urchin particles enlarge the particles' surface area and therefore the filler-matrix interface than in the case of the little bit branched necklace alloy chains. Accordingly, stronger filler-matrix interactions and thus more efficient stress transfer evolve between the two phases in UMB2-SU PNC than in UMB2-NL one.

| Sample | Relative Modulus | Relative yield strength | Relative strain at yield (%) | Relative Strain at break (%) |
|---|---|---|---|---|
| UMB0 | 1 ± 0.04 | 1 ± 0.02 | 1 ± 0.07 | 1 ± 0.15 |
| UMB2-SU | 1.13 ± 0.02 | 1.12 ± 0.007 | 1 ± 0.02 | 0.54 ± 0.1 |
| UMB2-NL | 1.08 ± 0.01 | 1.07 ± 0.025 | 1.02 ± 0.03 | 0.41 ± 0.1 |

**Table 2.** Relative tensile properties of $Fe_{20}Ni_{80}$/PA6 PNCs

*3.4 Structural analyses of $Fe_{20}Ni_{80}$/PA6 PNCs*

The DSC melting and crystallization thermograms have been used to characterize the degree of crystallinity ($X_C$), melting ($T_m$) and crystallization temperatures ($T_c$) of neat PA6 and the nanocomposites. The data are listed in Table3.

| Sample | $X_C$ (%) | $T_m$ (°C) | $T_c$ (°C) |
|---|---|---|---|
| UMB0 | 32.5 | 224 | 198.5 |
| UMB2-SU | 38.5 | 223 | 199.5 |
| UMB2-NL | 37 | 222.5 | 199 |

**Table 3.** DSC data for PA6 and $Fe_{20}Ni_{80}$/PA6 PNCs

Upon analyzing the DSC data, it is noted that UMB2-SU and UMB2-NL PNCs have significantly higher $X_C$ and slightly higher $T_c$ of PA6 phase, compared to the neat PA6. The increased $T_c$ of PA6 phase in both nanocomposites indicates that the nc $Fe_{20}Ni_{80}$ particles act as effective nucleating agent, thus allowing the PA6 crystallization to start earlier and inducing the rate of crystallization leading eventually to increased degree of crystallinity. The synergy of the $X_C$ and $T_c$ for UMB2-SU as compared to UMB2-NL is an evidence for the improved filler-matrix interfacial interactions, when the nc $Fe_{20}Ni_{80}$ alloy exhibit the spherical-sea urchin architecture rather than the necklace one. In addition, it is one of the possible reasons for the synergy of tensile modulus and strength of UMB2-SU PNC, compared to UMB2-NL one.

XRD patterns for neat PA6 and the nanocomposites are presented in Figure 4. The peaks around $2\theta \approx 20°$ and 23° are assigned to $\alpha 1$ and $\alpha 2$ crystal planes of PA6, respectively while the peaks around $2\theta \approx 10°$ and 21° are assigned to $\gamma 1$ and $\gamma 2$ crystal planes of PA6, respectively [13]. The observed peaks around ($2\theta$ = 44°, 51°, 75°) are attributed to the disordered FCC γ-Fe-Ni taenite phase, as mentioned before in section 3.1.

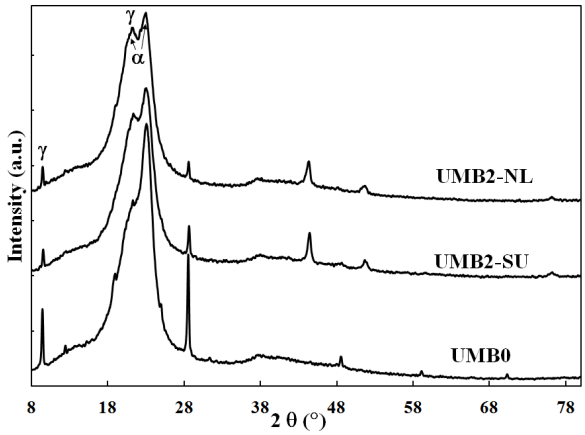


**Figure 4.** XRD pattern for PA6 and $Fe_{20}Ni_{80}$/PA6 PNCs

It is noticed that the nanocomposites exhibit increased relative fraction of γ-form to α-form PA6 crystals, compared to neat PA6. Thus the PA6 γ phase (%) measures 20%, 26% and 41% for neat PA6, UMB2-SU and UMB2-NL PNCs, respectively. The lower $T_m$ of PA6 phase, according to the DSC analyses, is in agreement with the increased PA6 γ phase (%), based on the XRD analyses, within the nanocomposites as compared to neat PA6, indicating that less ordered PA6 crystals are favored in the presence of nc $Fe_{20}Ni_{80}$ particles. It is speculated that the nc $Fe_{20}Ni_{80}$ particles disturb the PA6 crystals while being formed during the crystallization process, leading to the profusion of less ordered γ-phase crystals in the PNCs as compared to neat PA6. The disturbance of PA6 crystalline order is higher in UMB2-NL PNC than in UMB2-SU PNC, as evidenced from $T_m$ and γ phase (%) values. This is probably because the nc $Fe_{20}Ni_{80}$ particles are larger in UMB2-NL PNC, owing to the worse dispersibility of necklace $Fe_{20}Ni_{80}$ agglomerates versus spherical-sea urchin $Fe_{20}Ni_{80}$ agglomerates. The increased γ phase (%) might be one reason for the smaller enhancement of stiffness and strength of UMB2-NL PNC compared to UMB2-SU one, relative to neat PA6.

## 4. Conclusions

nc $Fe_{20}Ni_{80}$ alloys of two different geometries, spherical-sea urchin like particles and necklace chains, were chemically synthesized by varying the concentration of metals' precursors in the reaction solution. Then $Fe_{20}Ni_{80}$/PA6 nanocomposites with various nanofiller geometries were made by compounding the materials via UMB process and injection molding. The tensile properties and physical structure of the produced PNCs were characterized. The results reveal that the addition of nc $Fe_{20}Ni_{80}$ particles to PA6 enhances modulus and strength at the expense of toughness and UMB2-SU PNC exhibits synergistic tensile properties as compared to UMB2-NL one. Based on structural and morphological analyses, the variant tensile behavior between nanocomposites is attributed to the considerable effect of nanofiller geometry on i) the dispersibility and surface area of alloy particles and ii) the crystallinity and relative fraction of γ-form to α-form crystals of PA6 phase, within the nanocomposites.

## References


[1] Y. Cao, S. G. Ai, J. Zhang, N. Gu, and S. Hu Template-free synthesis snd characterization of leaf-like Fe-Ni microstructures. *Advanced. Material. Letter*, 4 (2):160-163, 2013.

[2] E. L. Jr, V. Drago, R. Bolsoni, and P. F. P. Fichtner. Nanostructured $Fe_{50}$ $Ni_{50}$ alloy formed by chemical reduction. *Solid State Communications*, 125 (5):265-270, 2003.

[3] Y. M. Yeh, G. C. Tu, and T. H. Fang Nanomechanical properties of nanocrystalline Ni-Fe mold insert. *Journal of Alloys and Compounds*, 372 (1-2): 224-230, 2004.

[4] M. Mohamed, A. El-Maghraby, M. Abd EL-Latif, H. Farag and K. Kalaitzidou. Fe-Ni alloy/polyamide 6 nanocomposites: effect of nanocrystalline metal particles on the mechanical and physical properties of the polymer. *Journal of Polymer Research*, 20 (6):137-145, 2013.

[5] M. A. A. Mohamed, A. El-Maghraby, M. Abd EL-Latif, H. Farag and K. Kalaitzidou. Nanocrystalline Fe-Ni alloy/polyamide 6 composites of high mechanical performance made by ultrasound-assisted master batch technique. *Polymer Composites*, DOI: 10.1002/pc.22901, 2014.

[6] M. A. A. Mohamed. Morphology-Controlled Facial Synthesis and Magnetism of Nanocrystalline Fe-Ni alloy. *Submitted to Materials Science and Engineering: B*, (March, 2014).

[7] D. Ratna, S. Divekar, A. B. Samui, B. C. Chakraborty, and A. K. Banthia. Poly(ethylene oxide)/clay nanocomposite:Thermomechanical properties and morphology. *Polymer,* 47: 4068- 4074, 2006.

[8] Q. Wu, X. Liu, and L. A. Berglund. An unusual crystallization behavior in polyamide 6/montmorillonite nanocomposites. *Macromolecular Rapid Communications,* 22 (17): 1438-1440, 2001.

[9] L. Shen, I. Y. Phang, T. Liu. Nanoindentation studies on polymorphism of nylon 6. *Polymer Testing*, 25: 249–253, 2006.

[10] M. Ito, K. Mizuochi, and T. Kanamoto. Effects of crystalline forms on the deformation behaviour of nylon-6. *Polymer*, 39 (19): 4593-4598, 1998.

[11] R. Seltzer, P. M. Frontini, and Y-W. Mai. Effect of hygrothermal ageing on morphology and indentation modulus of injection moulded nylon 6/organoclay nanocomposites. *Composite Science and Technology,* 69: 1093-1100, 2009.

[12] B. D. Cullity. Elements of X-Ray Diffraction. Addison-Wesley Publishing Company, Inc,1956.

[13] X. Hu and X. Zhao. The effects of annealing (solid and melt) on the time evolution of the polymorphic structure of PA6/silicate nanocomposites. *Polymer,* 45: 3819-3825, 2004.